

Exceptional rings and non-Abelian topology in non-Hermitian high-spin systems

Peng-Zhen Sun(孙鹏震), Zhou-Tao Lei(雷周涛), and Yuan-Gang Deng(邓元刚)
Citation: Chin. Phys. B, 2025, 34 (**11**): 110303. DOI: 10.1088/1674-1056/addcbe
http://cpb.iphy.ac.cn; http://iopscience.iop.org/cpb

What follows is a list of articles you may be interested in

Non-quantized Zak phases, PT/APT symmetry transitions, and doubly degenerate exceptional points in a non-Hermitian spin-orbit coupled SSH model

Jun-Xing Huo(霍俊行), Jian Li(李健), Qing-Xu Li(李清旭), and Jia-Ji Zhu(朱家骥)
Chin. Phys. B, 2025, 34 (**7**): 070301. DOI: 10.1088/1674-1056/adc7f3

Disorder in parity-time symmetric quantum walks

Peng Xue(薛鹏)
Chin. Phys. B, 2022, 31 (**1**): 010311. DOI: 10.1088/1674-1056/ac3741

Two-body exceptional points in open dissipative systems

Peize Ding(丁霈泽) and Wei Yi(易为)
Chin. Phys. B, 2022, 31 (**1**): 010309. DOI: 10.1088/1674-1056/ac3396

High winding number of topological phase in non-unitary periodic quantum walk

Yali Jia(贾雅利) and Zhi-Jian Li(李志坚)
Chin. Phys. B, 2021, 30 (**10**): 100301. DOI: 10.1088/1674-1056/abf554

Anti-parity-time symmetric phase transition in diffusive systems

Pei-Chao Cao(曹培超) and Xue-Feng Zhu(祝雪丰)
Chin. Phys. B, 2021, 30 (**3**): 030505. DOI: 10.1088/1674-1056/abd694

Exceptional rings and non-Abelian topology in non-Hermitian high-spin systems

Peng-Zhen Sun(孙鹏震), Zhou-Tao Lei(雷周涛), and Yuan-Gang Deng(邓元刚)†

Guangdong Provincial Key Laboratory of Quantum Metrology and Sensing & School of Physics and Astronomy, Sun Yat-Sen University (Zhuhai Campus), Zhuhai 519082, *China*

(Received 19 March 2025; revised manuscript received 21 May 2025; accepted manuscript online 23 May 2025)

Topological phases featuring non-Abelian charges have garnered significant attention in recent years. In parallel, the study of multiband exceptional topology in non-Hermitian systems has emerged as a prominent research direction. In this study, we investigate a parity–time (PT) symmetric Hamiltonian, which hosts both conventional non-Abelian topological phases (NATPs) and hybrid phases. We propose an experimental scheme using spin-1 atoms with spin–orbit coupling trapped in two-dimensional (2D) lattices. Before adding a non-Hermitian term, we find the emergence of distinct topological phases mixed by two NATPs and establish their connection with NATPs theory. When a non-Hermitian term that preserves *PT* symmetry protection was introduced, stable second-order exceptional rings and third-order exceptional points emerge and they drive the edge states to manifest as discontinuous Fermi arcs in the surface Brillouin zone. However, with the variation of the non-Hermitian term, it is rather intriguing that two types of exceptional rings here transition from being internally tangent to externally tangent, transforming into a new topological phase equivalent to the Hermitian case. This research provides deeper insights into the nature of NATPs and the topological implications of exceptional structures, contributing to the field of topological physics.

Keywords: non-Abelian topology, parity–time symmetry, exceptional point, ultracold atoms

PACS: 03.65.Vf, 11.30.Er, 42.50.–p, 67.85.–d

DOI: 10.1088/1674-1056/addcbe **CSTR:** 32038.14.CPB.addcbe

1. Introduction

The field of topological physics has seen remarkable progress and the topological band theory developed from this has become one of the cornerstones in the search for novel quantum states of matter.[1–5] Topological states of matter possess non-trivial and robust properties, enabling breakthroughs across disciplines, from condensed matter physics[6–8] to quantum information processing.[9,10] Besides solid-state systems, topological states have also been validated in a variety of simulated systems such as cold atom systems,[11–20] photonic crystals,[21–25] and superconducting quantum circuits.[26–28] The prominent hallmark of topological phases is their topological invariants. Several approaches have been applied for classifying topological phases and establishing classification frameworks, such as Altland–Zirnbauer (AZ) symmetry classes[7,29–31] and symmetry indicator theory.[32] In this classification, the focus lies on Abelian topological invariants, such as Z (integer-valued) and Z_2 (binary-valued) types of invariants.[33–35]

As research on topological phases has become increasingly comprehensive, in the tangled multi-gap scenario, the conventional Abelian characterization becomes insufficient. To address this, the concept of non-Abelian topology has emerged.[36–40] For instance, in the presence of *PT* symmetry, multiband gaps can carry non-Abelian topological charges (NATCs)[36,41] and have richer topological phases.[39,42–44] In the topological semimetal with NATCs, the annihilation of degenerate points depends on the braiding path, and this behavior cannot be described by Abelian topological charges. Therefore, the quaternion, a non-Abelian topological charge, is introduced.[45–52] In non-Abelian topological insulators, exotic edge states emerge at the domain wall, determined by the non-Abelian topological charges on both sides of the system. This unique statistical behavior makes NATPs a promising platform for topological quantum computing.[9,53–55] Recent experiments have successfully realized NATPs and their braiding dynamics across various platforms.[13,39,43,45,46,51,56–59] In most cases, NATPs are protected by *PT* symmetry, making them particularly suitable for implementation in artificial quantum systems.

The *PT* symmetry also plays a central role in the recently emerging field of non-Hermitian physics. The *PT* symmetry ensures real eigenenergies within the *PT*-unbroken phase, thereby maintaining a balance between gain and loss and ensuring probability conservation.[60–63] And *PT* symmetry has significantly advanced the study of exceptional points (EPs),[24,64–75] where the eigenvalues and eigenstates coalesce. Recent studies have further revealed that *PT* symmetry, along with additional symmetries, can effectively reduce the codimension of EPs.[76–80] For example, while a second-order

†Corresponding author. E-mail: dengyg3@mail.sysu.edu.cn

© 2025 Chinese Physical Society and IOP Publishing Ltd. All rights, including for text and data mining, AI training, and similar technologies, are reserved.

exceptional point is generally stable in two-dimensional (2D) systems, it can exist in a one-dimensional (1D) system with *PT* symmetry as a boundary of *PT* symmetry breaking. The *PT* symmetry-protected real spectrum also prevents the occurrence of the non-Hermitian skin effect (NHSE)[17,50,81–95] in the bulk states, a phenomenon in which all eigenstates accumulate exponentially to the boundary due to the breakdown of conventional bulk–edge correspondence, providing a convenient platform for studying properties such as EPs in lattice systems.

In this study, we systematically explore *PT* symmetry-protected NATPs and the impact of exceptional structures based on high-spin ultracold atoms in 2D lattices. When the fundamental gap term of the system approaches zero, indicating proximity to NATPs boundary in the 1D limit,[41] the system becomes highly susceptible to external perturbations. So we observe a distinct critical behavior in the topological phase transition, where protected edge states are determined by NATCs arising from both the intrinsic system and spin–vector–momentum coupling perturbations in the other direction. And we also confirm the stability of the multiband bulk–edge correspondence in the non-critical regime, where the system's topological properties remain robust against perturbations.

In the 2D system, the *PT* symmetry can reduce the codimension of EPs, thereby enabling the observation of third-order exceptional points (EP3s) and exceptional rings (ERs). So when a non-Hermitian term that preserves *PT* symmetry protection was introduced, the ERs emerge in the system under two distinct energy gaps, and their intersection points are identified as EP3s. In other words, the system lacks point-gap topology but retains traditional line-gap topology. The disappearance of the NHSE also ensures that the observation of topological features, including degenerate points and edge states, remains free from interference. When the non-Hermitian (non-reciprocal hopping) strength is small, the two exceptional rings are tangent internally, and part of the topological phases transition into a trivial state, which is distinct from the Hermitian case. As the non-Hermitian strength increases, the two exceptional rings become tangent externally, surprisingly restores topological equivalence to the Hermitian case. Finally, we discovered discontinuous Fermi arcs linking different exceptional points across distinct exceptional rings.

This paper is organized as follows. Section 2 introduces the symmetrically protected model with a Raman-assisted spin–tensor–momentum coupling (STMC) term and derives the system Hamiltonian. Section 3 delves into the topological states, investigates the topological states, analyzes the properties of edge states, and presents a distinct bulk–edge correspondence. Section 4 introduces the symmetrically protected non-Hermitian term and examines the exceptional structures that can form, along with their influence on the bulk–edge correspondence. Finally, Section 5 provides a concise summary of our findings.

2. Model and Hamiltonian

In recent studies, the multi-band spin–tensor–momentum-coupled (STMC) ultracold atoms have been used to realize an unpaired triply degenerate point.[15,16,96–99] In the process of studying its 2D model, we have incorporated *PT* symmetric protection and a non-Hermitian term. We consider an ultracold gas of N fermionic atoms subjected to a bias magnetic field $\boldsymbol{B}$ along the quantization z axis. The atomic energy levels here involve three energy levels with spin-1 and excited states with $|0\rangle$ and $|\uparrow\rangle$. Then the fermionic atoms are deeply confined by the red-detuned 2D square optical lattices $\mathcal{U}(\boldsymbol{r}) = -U_{\rm ol}[\cos^2(k_{\rm L}x) + \cos^2(k_{\rm L}y)]$. Here $U_{\rm ol}$ is the depth of the optical lattice, and $k_{\rm L}$ is the wave vector of the laser for the optical lattice with $a = \pi/k_{\rm L}$ being the lattice constant. The atomic transition from the ground state $|\sigma(\sigma = \{\uparrow, 0\})\rangle$ to the excited state $|e_\sigma\rangle$ is driven by a pair of π-polarized standing wave lasers with Rabi frequencies $\Omega'_\pi \sin(k_{\rm L}x - k_{\rm L}y)$ and $\mathrm{i}\Omega'_\pi \sin(k_{\rm L}x + k_{\rm L}y)$, corresponding the atom-light detuning $\Delta = \omega_{\rm a} - \omega_{\rm L}$. So the spatially dependent total Rabi frequency is $\Omega_1(\boldsymbol{r}) = \Omega_\pi[\sin(k_{\rm L}x)\cos(k_{\rm L}y) + \mathrm{i}\cos(k_{\rm L}x)\sin(k_{\rm L}x)]$ with $\Omega_\pi = \sqrt{2}\,\mathrm{e}^{\mathrm{i}\pi/4}\Omega'_\pi$. To generate spin–orbit (SO) coupling, the atomic transitions $|0\rangle \leftrightarrow |e_\uparrow\rangle$ and $|\downarrow\rangle \leftrightarrow |e_0\rangle$ are driven by two σ-polarized plane-wave lasers propagating along z direction with the same Rabi frequency $\Omega_2(\boldsymbol{r}) = \Omega_3(\boldsymbol{r}) = \Omega_\sigma\,\mathrm{e}^{\mathrm{i}\sqrt{2}k_{\rm L}z}$ as shown in Fig. 1(a), where the laser frequency is $\omega_{\rm L} + \Delta\omega_{\rm L}$ and $\omega_{\rm L} - \Delta\omega'_{\rm L}$.

For large atom-light detuning Δ, two excited states can be adiabatically eliminated to yield a pseudospin-1 system. When the lattice potential is sufficiently strong, the system enters the tight-binding regime. By only considering the lowest s orbits and nearest-neighbor hopping as shown in Figs. 1(b) and 1(c), the lattice Hamiltonian is given by

$$\begin{aligned} H_0 = &-\sum_{\boldsymbol{j},\alpha=x,y}[\mathrm{i}t_0\hat{\psi}^\dagger_{\boldsymbol{j}}\hat{F}_\alpha\hat{\psi}_{\boldsymbol{j}+1_\alpha} + t\hat{\psi}^\dagger_{\boldsymbol{j}}(2\hat{F}_z^2 - \hat{I})\hat{\psi}_{\boldsymbol{j}+1_\alpha} + \mathrm{H.c.}] \\ &+\sum_{\boldsymbol{j}}[(\delta+\delta_2)\hat{n}_{\boldsymbol{j},\uparrow} - (\delta-\delta_2)\hat{n}_{\boldsymbol{j},\downarrow}], \end{aligned} \tag{1}$$

where $\hat{\psi}_{\boldsymbol{j}} = [\hat{a}_{\boldsymbol{j},\uparrow}, \hat{a}_{\boldsymbol{j},0}, \hat{a}_{\boldsymbol{j},\downarrow}]^{\rm T}$ and $\hat{n}_{\boldsymbol{j},\sigma} = \hat{a}^\dagger_{\boldsymbol{j},\sigma}\hat{a}_{\boldsymbol{j},\sigma}$ with $\hat{a}_{\boldsymbol{j},\sigma}$ being the annihilation operator for spin-σ compoment in the $\boldsymbol{j}$ site, t_0 is Raman-assisted spin-flip hopping, t is spin-independent hopping and $\delta(\delta_2)$ is the effective tunable linear (quadratic) Zeeman shift. Here the unit vectors along two directions are defined by $\mathbf{1}_x = (1,0)$ and $\mathbf{1}_y = (0,1)$.

We consider constructing the entire Hamiltonian satisfies *PT* symmetry, which transforms the F_y term into $Q_{xz} = F_xF_z + F_zF_x$, and introduce a non-Hermitian term to investigate the exceptional structures. Under periodic boundary condition

with translational invariance, the Hamiltonian (1) in momentum space takes the form

$$H(\boldsymbol{k}) = d_x(\boldsymbol{k})\hat{F}_x + d_y(\boldsymbol{k})\hat{Q}_{xz} + \delta\hat{F}_z + d_z'(\boldsymbol{k})\hat{F}_z^2 + \epsilon(\boldsymbol{k})\hat{I} + \mathrm{i}\gamma\hat{F}_y, \tag{2}$$

where $d_x(\boldsymbol{k}) = 2t_0\sin(k_x a)$, $d_y(\boldsymbol{k}) = 2t_0\sin(k_y a)$, $d_z'(\boldsymbol{k}) = (\delta_2 - 4t\cos(k_x a) - 4t\cos(k_y a))$, and $\epsilon(\boldsymbol{k}) = 2t(\cos(k_x a) + \cos(k_y a))$. Obviously, the first term $d_\alpha(\boldsymbol{k})F_\alpha$ represents the conventional spin–vector–momentum-coupled (SVMC) term, and the term $d_z'(\boldsymbol{k})F_z^2$ represents the interesting STMC for our high-spin system. Only when the non-Hermitian term is $\mathrm{i}\gamma F_y$, is the PT symmetry satisfied and it is the nonreciprocal hopping term between $|0\rangle$ and $|\uparrow,\downarrow\rangle$.

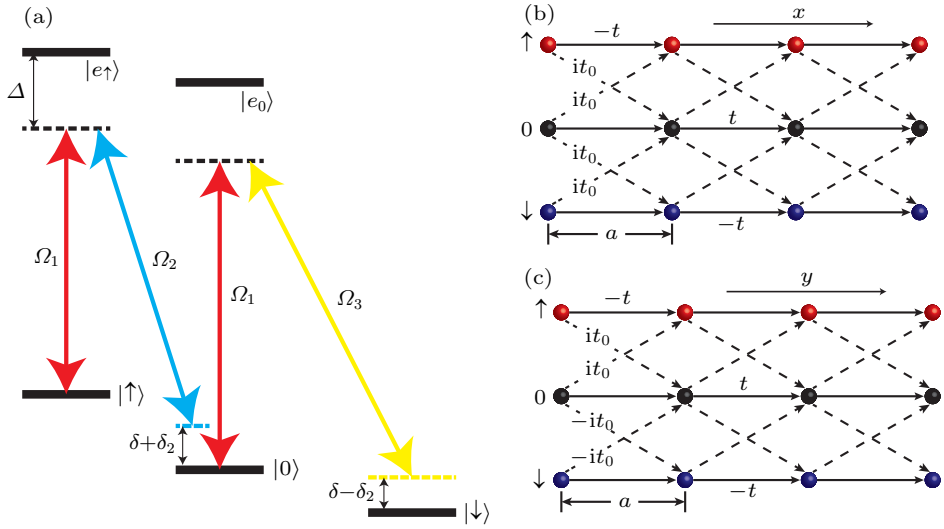


Fig. 1. (a) Involved level structure for creating STMC for ultracold atoms, (b) the lattice model along x direction, (c) the lattice model along y direction.

3. Non-Abelian topology and edge states

To further characterize the non-Abelian topology of the system, we first calculate the energy spectrum in momentum space and the NATCs in the absence of the non-Hermitian term. There we calculate the energy spectrum in momentum space via $H(\boldsymbol{k})|\mu_\alpha(\boldsymbol{k})\rangle = E_\alpha(\boldsymbol{k})|\mu_\alpha(\boldsymbol{k})\rangle$, where $E_\alpha(\boldsymbol{k})[|\mu_\alpha(\boldsymbol{k})\rangle]$ denotes the eigenenergies (eigenstates) with $\alpha = \{-,0,+\}$ indexing the {lowest, middle, highest}-helicity branches, respectively. Due to its interband degeneracy, the system must be described by at least three topological charges, each associated with every two bands. These charges are braided with each other, representing a concept that is fundamentally distinct from the Berry phase typically used to characterize the topology of a single bandgap. And guaranteed by PT symmetry, the eigenvectors of this system are purely real under a specific basis, satisfying one of the conditions for non-Abelian charges. However, for the 1D non-Abelian charges, the tunable linear Zeeman shift term $\delta = 0$ corresponds to the junction of different non-Abelian charges. Therefore, we select a smaller value to study the critical behavior and choose an appropriate value to investigate the bulk–edge correspondence

Clearly, this Hamiltonian possesses PT symmetry, expressed as $(PT)H(k_x,k_y)(PT)^{-1} = H^*(k_x,k_y)$ where $PT = \kappa I$ with κ being the complex-conjugate operator. When the non-Hermitian term is zero, it additionally exhibits both time-reversal symmetry and spatial inversion symmetry, with their operators represented as $\mathrm{e}^{-\mathrm{i}\pi\hat{F}_z}$. However, the introduction of the non-Hermitian term breaks time-reversal (T) symmetry and spatial inversion (P) symmetry while preserving their combined PT symmetry. For simplicity, we set $t_0 = t$, since the non-Abelian topological phase boundary is independent of nonzero t_0/t. Thus the free parameters in our model reduce to the tunable linear Zeeman shift δ, quadratic Zeeman shift δ_2 and the non-Hermitian term γ.

of the non-Abelian charge. We use the non-Abelian charges to simplify them into four forms of topological charges[41,43] and is described by

$$Q = \overline{\exp}\left[\oint A(k_x)\cdot \mathrm{d}k_x\right], \tag{3}$$

where $A(k_x) = \sum_t \beta_t[-(\mathrm{i}/2)\sigma_t]$ with σ_t as the Pauli matrix, which is from the affine Berry–Wilczek–Zee (BWZ) connection, $\beta_t = \sum_{pq}\langle\mu_p(k_x)|\partial_{k_x}|\mu_q(k_x)\rangle\epsilon_{tpq}/2$ calculated from bands p and q, ϵ_{tpq} being the antisymmetric tensor. The bar over the exponent indicates path ordering, which denotes that the integration is time-ordered, and during discrete numerical treatment each discretized point should be right-multiplied by Q by order. This essentially describes the generalized Wilson operator as an $\mathfrak{so}(N)$-valued 1-form transforming into a $\mathfrak{spin}(N)$-valued 1-form.[3,43] Here the results of quaternion group elements are represented as Pauli matrix $1 \to \sigma_0, i \to \mathrm{i}\sigma_x, j \to \mathrm{i}\sigma_y$, and $k \to \mathrm{i}\sigma_z$, where σ_0 is the 2×2 identity matrix. And the signs $\pm$ only have the relative meaning for NATCs, i, j, and k. Only 1 represents the trivial phase and has no edge states. The charge of $i(k)$ indicates the second (first) gap is nontrivial and supports one edge state on each

end of a finite-length lattice. The charge of j indicates that there are left and right local edge states in the middle of the second band, or there are two left and right local edge states in the first and second energy gaps. By contrast, the charge of -1 supports two edge states on each edge and the locations of the edge states are fickle. This phase transition is often accompanied by the exchange of energy bands, which closes and reopens the energy gap. $\pm i(\pm j, \pm k)$ can only be distinguished to a basepoint, which means that a pair of conjugate charges cannot be distinguished by observing them separately. They only show differences at the boundaries.[36,39,41,43–45]

Specifically, in two (three)-dimensional systems, non-Abelian topological charges can be understood as degeneracy points (lines) in momentum space, with their topology characterized by 1D loops encircling these points (lines). Here, the charge $+i$ signifies the non-trivial topology of the second bandgap (corresponding to a degeneracy point between the second and third bands), while $+k$ represents the non-trivial topology of the first energy gap (associated with a degeneracy between the first and second bands). When some parameter is varied, these two points may form trajectories that cross each other corresponding to two exchanges between $+i$ and $+k$, leading to transformations such as $+k \to iki^{-1} = -k$. This process resembles the braiding of strands in a rope, so we topologically call it braiding with each other. Therefore, their non-Abelian nature manifests as non-commutativity ($k \times i \neq i \times k$) and path-dependent outcomes. Compared to Abelian charges, which only exhibit simple annihilation/creation processes, the non-Abelian topological charge greatly enriches and describes the more complex winding relationship and more complex bulk–edge correspondence rules of the multi-band system. It not only records the geometry of band crossing, but also determines the global history of quantum state evolution.[45,52]

Here we can calculate the NATCs in the 1D x-direction from our model. When we remove the momentum-coupling term $d_y(\boldsymbol{k})\hat{Q}_{xz}$ in the y-direction as a perturbation term, the entire Hamiltonian is $H_x(k_x)$ in the form of a 1D system in the x-direction. This Hamiltonian $H_x(k_x)$ precisely matches the form required to calculate NATCs, similar to the standard 1D non-Abelian model.[41] This model directly satisfies the 1D non-Abelian bulk–edge correspondence, with $\delta = 0$ marking the transition boundary between different non-Abelian charges. Therefore, we choose δ as a very small value to obtain the distribution of its NATCs under the parameters $k_y a/\pi$ and δ_2/t, as shown in Fig. 2(a). The middle wave-like region in the figure corresponds to the topologically nontrivial phase characterized by the non-Abelian charge $-j$. The analytic boundary for the NATPs is given by $\delta_2/t = 4\cos(k_y a) \pm 4$, where a band inversion occurs between energy bands 1 and 3. This result reflects the undisturbed distribution of NATCs in the x-direction for the parameters $k_y a/\pi$ and δ_2/t. Furthermore, the distribution of edge states is fully consistent with this result. However, when we introduce the SVMC perturbation in the y-direction, the original distribution is partially disrupted, leading to the partial disappearance of the edge states as shown in Fig. 2(b). When δ is non-zero, the region distribution corresponding to the $-j$ charge exhibits robustness against variations in δ. An increase in δ only alters the $i(k)$ charge region, while the $-j$ region remains largely unchanged, still concentrated in the ranges of $(0, 0\text{–}8)$ and $(\pm 1, -8\text{–}0)$. The combination of these two results ultimately establishes the model's bulk–edge correspondence.

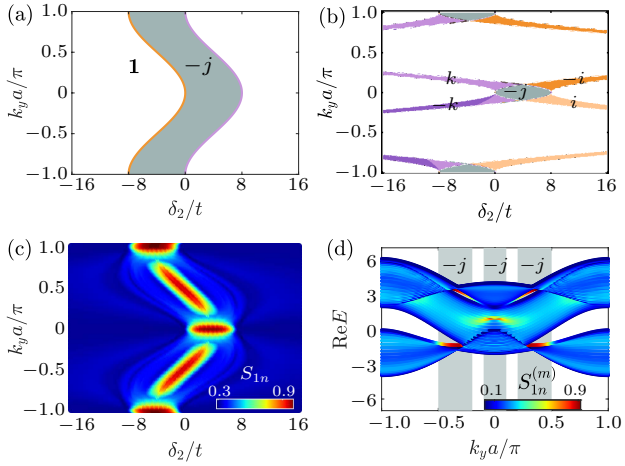


Fig. 2. NATCs and edge states result on the $k_y a$–δ_2 plane, (a) the NATCs result of $H_x(k_x)$, (b) the NATCs result with y-direction perturbation added, (c) the distribution of S_{1n} under all $k_y a$ and δ_2 parameters, (d) the distribution of $S_{1n}^{(m)}$ along x direction with parameters $\delta_2/t = 2$. The other parameters are $\delta/t = 0.2$ and $\gamma = 0$.

Assuming that the system has N lattice along the x direction, we can determine the corresponding lattice energy and eigenstate distributions under different parameters. We use the maximum value S_{1n} of the sum $S_{1n}^{(m)}$, which represents the sum of the squared amplitudes of the eigenstate wavefunctions at the two boundaries (1 and n) corresponding to the m-th of $3N$ energy levels under the parameters δ_2/t and $k_y a/\pi$, as quantitative measures of the edge states. In the end, we obtain the map of S_{1n} as shown in Fig. 2(c), which reflects the combined result of these NATCs results. As δ increases from zero, it progressively compresses all regions except the robust ones $(0, 0\text{–}8)$ and $(\pm 1, -8\text{–}0)$, which gradually diminish. Crucially, the strip-shaped $i(k)$ region here is due to computational errors caused by the critical region, which has no effect on the edge states. Here, the $-j$ charge in the robust regions indicates that the edge states merge into the second continuum band, forming bound-states-in-continuum (BICs). Specifically, the edge states are localized at the center of the lattice's energy spectrum. And the $-j$ charge in other regions corresponds to the generic bulk–edge result of the aforementioned j case. It represents the metastable existence of $-j$ charges near the $\delta = 0$ critical point in the absence of y-direction perturbations. These $-j$ charges gradually annihilate as δ increases. Therefore, the critical behavior emerges from the interplay between these two

competing topological charges. When we fix the parameter $\delta_2/t = 2$, we observe the $-j$ phase, where edge states emerge in two energy gaps, with the $-j$ phase transitions into BICs in the intermediate region, as illustrated in Fig. 2(d).

When δ is sufficiently large (e.g., $\delta/t = 2$), the influence of NATCs induced by the perturbation term becomes significant. Consequently, the edge states in the unperturbed x-direction disappear, and the results align with the bulk–edge correspondence of NATCs. These finding are illustrated in the Fig. 3. We calculate NATCs and find that they transition through the $-i$, $-j$, and k phases as the parameter δ_2/t varies. Additionally, the NATCs depends on δ_2/t and change with the parameter $k_y a/\pi$. By setting $k_y = 0$, we identify the topological phase transitions through the three phases $-i$, $-j$, and k as shown in Fig. 3(c). Here, the $-i$ charge indicates that the second energy gap is topologically nontrivial and supports one edge state an each end of a finite-length lattice, while the k charge corresponds to a nontrivial first energy gap with the edge states localized within the first energy gap. However, for the j charge, the edge states are located in both the first and second energy gaps. This represents a general case that is distinct from the behavior of BICs. The non-Abelian topological phases $-i$, $-j$, and k are illustrated in Fig. 3(a). When we fix the parameter $\delta_2/t = 0$, we also observe the distribution of the corresponding topological edge states, as shown in Fig. 3(d). This distribution is fully consistent with the NATCs mapping.

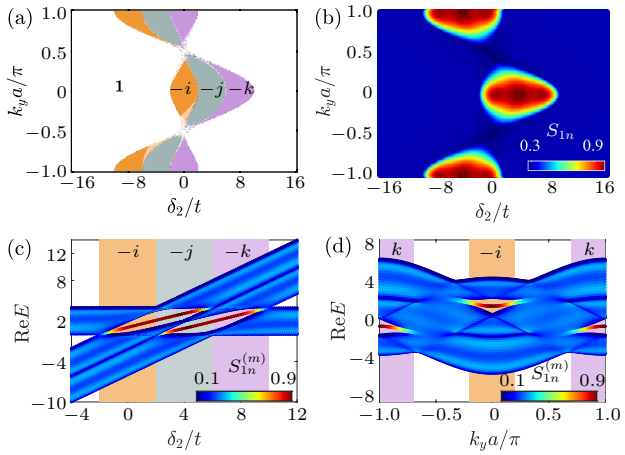


Fig. 3. NATCs and edge states result on the $k_y a$–δ_2 plane: (a) the non-Abelian topological phases, (b) the distribution of locality under all $k_y a$ and δ_2/t parameters, (c) edge states along x direction through the $-i$, $-j$, k phases with parameters $k_y a/\pi = 0$ of all edge states, (d) edge states along x direction through the k, $-i$, k phases with parameters $\delta_2/t = 0$ of all edge states. The other parameters are $\delta/t = 2$ and $\gamma = 0$.

4. Exceptional structures protected by *PT* symmetry

When we introduce the non-Hermitian term ($\gamma \neq 0$) that preserves *PT* symmetry protection, the line gap remains open in the *PT* unbroken region, so we can still use NATCs to determine the topological charge based on the position of edge states. And the system exhibits EP3s and ERs due to the influence of symmetry protection. Their distribution is symmetric about the origin. To investigate the distribution of exceptional structures, we calculate the energy spectrum by analyzing the Hamiltonian in Eq. (2). Under *PT* symmetry, the system may exhibit EP3s. To ensure the inevitable occurrence of EP3s, we must verify that additional symmetry protection exists under specific parameters. Here, we set $\delta = 0$ and remove the STMC term, leaving the entire model protected by chiral symmetry, represented by the operator $e^{-i\pi\hat{F}_z}$. Under this symmetry, a third-order ER emerges at the position $d_x^2 + d_y^2 = \gamma^2$. From this analysis, we conclude that the necessary conditions for the existence of EP3s are $d_z' = 0$ and the formation of the exceptional ring.

Additionally, we adopt the method of symmetry-induced EPs,[80] which utilizes Gell–Mann matrices to describe the system. We introduce

$$\nu = \det[H]/2 \text{ and } \eta = -\mathrm{tr}[H^2]/6, \tag{4}$$

such that characteristic polynomial can be expressed as $P_3 = \epsilon^3 + 3\eta\epsilon - 2\nu$ and the discriminant for degeneracies is $D_3 = -108(\eta^3 + \nu^2) = 0$. An EP3 occurs when $\nu = \eta = 0$, while EP2s appear when $D_3 = 0$. Here, the identity matrix does not affect the Hamiltonian; so we introduce a specific identity matrix to ensure the trace of the Hamiltonian is zero, simplifying the calculations. Under this condition, we find that EP3s correspond to the ring defined by $d_x^2 + d_y^2 = \gamma^2$ and $d_z' = 0$, while the ERs correspond to either the same ring or the term $d_z'^2/4$ preceding it.

We set $\delta = 0$ and $\delta_2 = 0$, and as γ^2 varies from 0 to $8t^2$, the EP3s remain present, while the relative positions of the ERs undergo significant changes. From the relative positions of these two ERs, we identify two distinct structural configurations. When $0 < \gamma < 2t$, the two distinct ERs are internally tangent, and the adjacent EP3s are connected by these rings, ultimately forming a closed structure. Within one cycle, there exist two such structures. To facilitate the description of the edge state distribution, We use the same maximum value S_{1n} and the same sum $S_{1n}^{(m)}$ under the parameters δ_2/t and $k_y a/\pi$ as quantitative measures of the edge states. In this scenario, the two exceptional rings are internally tangent, forming a closed exceptional structure. When expanded along the x-direction, the *PT*-unbroken region manifests as a degeneracy in the imaginary part of the spectrum. Here, the original topological edge states do not completely vanish but persist in the middle regions ($k_y/\pi = \pm 1/2$) between the two sides. And more are affected by the asymmetric non-Hermitian skin effect, resulting in edge states appearing on one side, while no edge states appear on the other side. Therefore, this leads to a transition where the originally bilateral edge states become localized on one side, either at both ends or collapsing toward the central

part of that side. When the non-Hermitian term is small, the formation of closed exceptional structure leads to the collapse of the edge states as shown in Figs. 4(a) and 4(b).

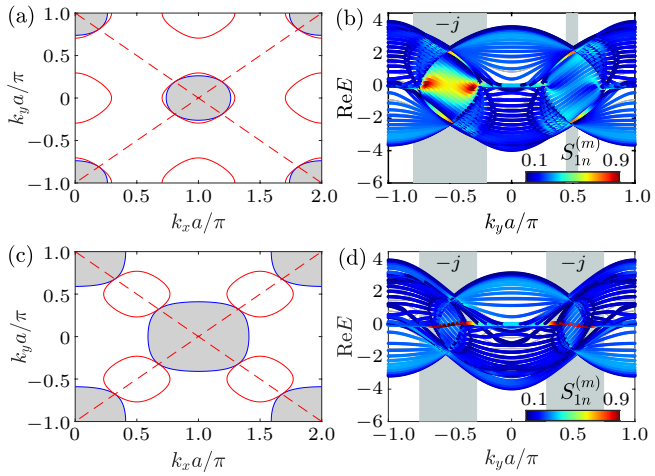


Fig. 4. Two different exceptional structures and the corresponding edge states with parameters $\delta = 0$ and $\delta_2 = 0$: panels (a) and (b) are the isolate ERs result and the corresponding edge states that unfold along x-direction distribution with parameter $\gamma/t = 1.6$. Panels (c) and (d) are the connected ERs result and the corresponding edge states that unfold along x-direction distribution with parameter $\gamma/t = 2.4$. The red and blue ring is the ERs and the red dotted line is $d_z' = 0$ and the gray area is the PT-broken region. The color represents the sum of the squared amplitudes of the eigenstate wavefunctions at the two boundaries.

When $\gamma > 2t$, one of the two ERs undergoes coupling-induced non-Hermitian phase transition, arising from the competition between the spin–tensor–momentum coupling term and the non-Hermitian potential. So the two distinct exceptional rings are externally tangent, with their adjacent EP3s linked either by a segment of an exceptional ring or by an entire exceptional ring, ultimately forming a network-like connected structure as shown in Fig. 4(c). This network-like structure ensures a uniform distribution of the exceptional rings. When the system is expanded along x-direction, the PT-unbroken region will give rise to two new energy bands above and below the imaginary part of the spectrum, which are caused by the emergence of the one ER. So each band has degenerate energy states, causing the edge states to be concentrated within these two bands, and the skin effect disappears. Therefore, in one dimension, the edge states no longer collapse but instead merge into the second continuum band in the unbroken PT-symmetric regime, forming the j-phase of bound states in the continuum as shown in Fig. 4(d). As a result, the system instead reverts to a state that is topologically equivalent to the 1D unperturbed NATPs, as shown in Fig. 2(a), and the corresponding topological charge is j.

5. Conclusion

Building upon state-of-the-art techniques for ultracold atoms, we proposed a 2D spin-1 lattice model, which exhibits symmetry-protected topological phases under PT symmetry. This multi-band system exhibits a distinctive bulk–edge correspondence, which necessitates both NATCs characterization and a perturbative treatment of spin–vector–momentum coupling near the boundary of the NATPs, revealing critical behavior. And we also verify the existence of a non-Abelian bulk–edge correspondence phase under non-critical conditions, where perturbations are applied in a different direction. In addition, the introduction of a non-Hermitian term that preserves PT symmetry induces stable ERs and EP3s. As the non-Hermitian term varies, the exceptional rings transition from internally tangent to externally tangent, leading to a new phase topologically equivalent to the Hermitian case. Our findings deepen the understanding of non-Abelian topological physics and establish a theoretical framework for manipulating topological states via exceptional point engineering. The proposed experimental platform provides a viable route for observing these exotic topological phenomena, paving the way for exploring non-Hermitian topological matter and its potential applications in quantum technologies.

Acknowledgement

Project supported by the National Natural Science Foundation of China (Grant Nos. 12274473 and 12135018).

References

[1] Zhang H, Liu C X, Qi X L, Dai X, Fang Z and Zhang S C 2009 *Nat. Phys.* **5** 438
[2] Hasan M Z and Kane C L 2010 *Rev. Mod. Phys.* **82** 3045
[3] Qi X L and Zhang S C 2011 *Rev. Mod. Phys.* **83** 1057
[4] Vergniory M G, Elcoro L, Felser C, Regnault N, Bernevig B A and Wang Z 2019 *Nature* **566** 480
[5] Zhang T, Jiang Y, Song Z, Huang H, He Y, Fang Z, Weng H and Fang C 2019 *Nature* **566** 475
[6] Xiao D, Chang M C and Niu Q 2010 *Rev. Mod. Phys.* **82** 1959
[7] Chiu C K, Teo J C Y, Schnyder A P and Ryu S 2016 *Rev. Mod. Phys.* **88** 035005
[8] Haldane F D M 1988 *Phys. Rev. Lett.* **61** 2015
[9] Nayak C, Simon S H, Stern A, Freedman M and Das Sarma S 2008 *Rev. Mod. Phys.* **80** 1083
[10] Lutchyn R M, Sau J D and Das Sarma S 2010 *Phys. Rev. Lett.* **105** 077001
[11] Goldman N, Budich J C and Zoller P 2016 *Nat. Phys.* **12** 639
[12] Song B, Zhang L, He C, Poon T F J, Hajiyev E, Zhang S, Liu X J and Jo G B 2018 *Sci. Adv.* **4** aao4748
[13] H M B, Boguslawski M, Barrios M, Xin L and Chapman M S 2019 *Phys. Rev. Lett.* **123** 173202
[14] Song B, He C, Niu S, Zhang L, Ren Z, Liu X J and Jo G B 2019 *Nat. Phys.* **15** 911
[15] Lei Z, Deng Y and Lee C 2020 *Phys. Rev. A* **102** 013301
[16] Lei Z, Deng Y and Lee C 2022 *Phys. Rev. Res.* **4** 033008
[17] Liang Q, Xie D, Dong Z, Li H, Li H, Gadway B, Yi W and Yan B 2022 *Phys. Rev. Lett.* **129** 070401
[18] Léonard J, Kim S, Kwan J, Segura P, Grusdt F, Repellin C, Goldman N and Greiner M 2023 *Nature* **619** 495
[19] Cornish S L, Tarbutt M R and Hazzard K R A 2024 *Nat. Phys.* **20** 730
[20] Zhao E, Wang Z, He C, Poon T F J, Pak K K, Liu Y J, Ren P, Liu X J and Jo G B 2025 *Nature* **637** 565
[21] Lu L, Joannopoulos J D and Soljačić M 2014 *Nat. Photon.* **8** 821
[22] Gross C and Bloch I 2017 *Science* **357** 995
[23] Raghu S and Haldane F D M 2008 *Phys. Rev. A* **78** 033834
[24] Cerjan A, Huang S, Wang M, Chen K P, Chong Y and Rechtsman M C 2019 *Nat. Photon.* **13** 623
[25] Miri M A and Alù A 2019 *Science* **363** eaar7709

[26] Barends R, Kelly J, Megrant A, Veitia A, Sank D, Jeffrey E, White T C, Mutus J, Fowler A G, Campbell B, Chen Y, Chen Z, Chiaro B, Dunsworth A, Neill C, O'Malley P, Roushan P, Vainsencher A, Wenner J, Korotkov A N, Cleland A N and Martinis J M 2014 *Nature* **508** 500

[27] Satzinger K J, Liu Y J and Smith A E 2021 *Science* **374** 1237

[28] Semeghini G, Levine H, Keesling A, Ebadi S, Wang T T, Bluvstein D, Verresen R, Pichler H, Kalinowski M, Samajdar R, Omran A, Sachdev S, Vishwanath A, Greiner M, Vuletić V and Lukin M D 2021 *Science* **374** 1242

[29] Altland A and Zirnbauer M R 1997 *Phys. Rev. B* **55** 1142

[30] Ryu S, Schnyder A P, Furusaki A and Ludwig A W W 2010 *New J. Phys.* **12** 065010

[31] Zhao Y X, Chen C, Sheng X L and Yang S A 2021 *Phys. Rev. Lett.* **126** 196402

[32] Tang F, Po H C, Vishwanath A and Wan X 2019 *Nature* **566** 486

[33] Thouless D J, Kohmoto M, Nightingale M P and den Nijs M 1982 *Phys. Rev. Lett.* **49** 405

[34] Kane C L and Mele E J 2005 *Phys. Rev. Lett.* **95** 226801

[35] Schnyder A P, Ryu S, Furusaki A and Ludwig A W W 2008 *Phys. Rev. B* **78** 195125

[36] Wu Q, Soluyanov A A and Bzdušek T 2019 *Science* **365** 1273

[37] Ahn J, Park S and Yang B J 2019 *Phys. Rev. X* **9** 021013

[38] Bouhon A, Bzdušek T and Slager R J 2020 *Phys. Rev. B* **102** 115135

[39] Jiang B, Bouhon A, Lin Z K, Zhou X, Hou B, Li F, Slager R J and Jiang J H 2021 *Nat. Phys.* **17** 1239

[40] Guo C X, Chen S, Ding K and Hu H 2023 *Phys. Rev. Lett.* **130** 157201

[41] Sun X C, Wang J B, He C and Chen Y F 2024 *Phys. Rev. Lett.* **132** 216602

[42] Ünal F N, Bouhon A and Slager R J 2020 *Phys. Rev. Lett.* **125** 053601

[43] Guo Q, Jiang T, Zhang R Y, Zhang L, Zhang Z Q, Yang B, Zhang S and Chan C T 2021 *Nature* **594** 195

[44] Li T and Hu H 2023 *Nat. Commun.* **14** 6418

[45] Bouhon A, Wu Q, Slager R J, Weng H, Yazyev O V and Bzdušek T 2020 *Nat. Phys.* **16** 1137

[46] Wang K, Dutt A, Wojcik C C and Fan S 2021 *Nature* **598** 59

[47] Hu H and Zhao E 2021 *Phys. Rev. Lett.* **126** 010401

[48] Chen Z G, Zhang R Y, Chan C T and Ma G 2021 *Nat. Phys.* **18** 179

[49] Patil Y S S, Höller J, Henry P A, Guria C, Zhang Y, Jiang L, Kralj N, Read N and Harris J G E 2022 *Nature* **607** 271

[50] Rui W B, Zhao Y X and Wang Z D 2023 *Phys. Rev. B* **108** 165105

[51] Zhang Q, Li Y, Sun H, Liu X, Zhao L, Feng X, Fan X and Qiu C 2023 *Phys. Rev. Lett.* **130** 017201

[52] Xu S, Sun Z Z, Wang K and Li E A 2024 *Nat. Phys.* **20** 1469

[53] Alicea J 2012 *Rep. Prog. Phys.* **75** 076501

[54] Stern A and Lindner N H 2013 *Science* **339** 1179

[55] Field B and Simula T 2018 *Quantum Science and Technology* **3** 045004

[56] Ni X, He C, Sun X C, Liu X P, Lu M H, Feng L and Chen Y F 2015 *New J. Phys.* **17** 053016

[57] Wang D, Yang B, Wang M, Zhang R Y, Li X, Zhang Z Q, Zhang S and Chan C T 2022 *Phys. Rev. Lett.* **129** 263604

[58] Wang M, Liu S, Ma Q, Zhang R Y, Wang D, Guo Q, Yang B, Ke M, Liu Z and Chan C T 2022 *Phys. Rev. Lett.* **128** 246601

[59] Hu Y, Tong M, Jiang T, Jiang J H, Chen H and Yang Y 2024 *Nat. Commun.* **15** 10036

[60] Bender C M and Boettcher S 1998 *Phys. Rev. Lett.* **80** 5243

[61] Mostafazadeh A 2002 *J. Math. Phys.* **43** 205

[62] Feng L, El-Ganainy R and Ge L 2017 *Nat. Photon.* **11** 752

[63] El-Ganainy R, Makris K G, Khajavikhan M, Musslimani Z H, Rotter S and Christodoulides D N 2018 *Nat. Phys.* **14** 11

[64] Heiss W D 2004 *J. Phys. A: Math. Gen.* **37** 2455

[65] Dembowski C, Dietz B, Gräf H D, Harney H L, Heine A, Heiss W D and Richter A 2004 *Phys. Rev. E* **69** 056216

[66] Hassan A U, Zhen B, Soljačić M, Khajavikhan M and Christodoulides D N 2017 *Phys. Rev. Lett.* **118** 093002

[67] Budich J C, Carlström J, Kunst F K and Bergholtz E J 2019 *Phys. Rev. B* **99** 041406

[68] Zhou H and Lee J Y 2019 *Phys. Rev. B* **99** 235112

[69] Yoshida T, Peters R, Kawakami N and Hatsugai Y 2019 *Phys. Rev. B* **99** 121101

[70] Okugawa R and Yokoyama T 2019 *Phys. Rev. B* **99** 041202

[71] Tang W, Jiang X, Ding K, Xiao Y X, Zhang Z Q, Chan C T and Ma G 2020 *Science* **370** 1077

[72] Liu W, Wu Y, Duan C K, Rong X and Du J 2021 *Phys. Rev. Lett.* **126** 170506

[73] Cayao J and Black-Schaffer A M 2023 *Phys. Rev. B* **107** 104515

[74] Wang K, Xiao L, Lin H, Yi W, Bergholtz E J and Xue P 2023 *Sci. Adv.* **9** 2375

[75] Wu Y, Wang Y, Ye X, Liu W, Niu Z, Duan C K, Wang Y, Rong X and Du J 2024 *Nat. Nanotechnol.* **19** 160

[76] Xu Y, Wang S T and Duan L M 2017 *Phys. Rev. Lett.* **118** 045701

[77] Höller J, Read N and Harris J G E 2020 *Phys. Rev. A* **102** 032216

[78] Delplace P, Yoshida T and Hatsugai Y 2021 *Phys. Rev. Lett.* **127** 186602

[79] Tang W, Ding K and Ma G 2023 *Nat. Commun.* **14** 6660

[80] Montag A and Kunst F K 2024 *Phys. Rev. Res.* **6** 023205

[81] Rotter I 2009 *J. Phys. A: Math. Theor.* **42** 153001

[82] Lee T E 2016 *Phys. Rev. Lett.* **116** 133903

[83] Leykam D, Bliokh K Y, Huang C, Chong Y D and Nori F 2017 *Phys. Rev. Lett.* **118** 040401

[84] Gong Z, Ashida Y, Kawabata K, Takasan K, Higashikawa S and Ueda M 2018 *Phys. Rev. X* **8** 031079

[85] Yao S and Wang Z 2018 *Phys. Rev. Lett.* **121** 086803

[86] Lee C H, Li L and Gong J 2019 *Phys. Rev. Lett.* **123** 016805

[87] Kawabata K, Sato M and Shiozaki K 2020 *Phys. Rev. B* **102** 205118

[88] Zhang K, Yang Z and Fang C 2020 *Phys. Rev. Lett.* **125** 126402

[89] Okuma N, Kawabata K, Shiozaki K and Sato M 2020 *Phys. Rev. Lett.* **124** 086801

[90] Li Y, Liang C, Wang C, Lu C and Liu Y C 2022 *Phys. Rev. Lett.* **128** 223903

[91] Zhu P, Sun X Q, Hughes T L and Bahl G 2023 *Nat. Commun.* **14** 720

[92] Schindler F, Gu K, Lian B and Kawabata K 2023 *PRX Quantum* **4** 030315

[93] Lin R, Tai T, Li L and Lee C H 2023 *Front. Phys.* **18** 53605

[94] Ma X R, Cao K, Wang X R, Wei Z, Du Q and Kou S P 2024 *Phys. Rev. Res.* **6** 013213

[95] Lei Z, Lee C H and Li L 2024 *Commun. Phys.* **7** 100

[96] Luo X W, Sun K and Zhang C 2017 *Phys. Rev. Lett.* **119** 193001

[97] Hu H, Hou J, Zhang F and Zhang C 2018 *Phys. Rev. Lett.* **120** 240401

[98] Li D, Huang L, Peng P, Bian G, Wang P, Meng Z, Chen L and Zhang J 2020 *Phys. Rev. A* **102** 013309

[99] Zhang M, Yuan X, Li Y, Luo X W, Liu C, Zhu M, Qin X, Zhang C, Lin Y and Du J 2022 *Phys. Rev. Lett.* **129** 250501